# Static stress interactions in extensional earthquake sequences: An example from the South Lunggar Rift, Tibet

**Article** *in* Journal of Geophysical Research Atmospheres · September 2012

DOI: 10.1029/2012JB009365

CITATIONS
11

READS
117

**3 authors:**

Isabelle Ryder
University of Liverpool
**46** PUBLICATIONS **771** CITATIONS
SEE PROFILE

Roland Burgmann
University of California, Berkeley
**430** PUBLICATIONS **13,208** CITATIONS
SEE PROFILE

Eric J Fielding
California Institute of Technology
**259** PUBLICATIONS **8,477** CITATIONS
SEE PROFILE

# Static stress interactions in extensional earthquake sequences: An example from the South Lunggar Rift, Tibet

Isabelle Ryder,[1] Roland Bürgmann,[2] and Eric Fielding[3]

Received 4 April 2012; revised 23 July 2012; accepted 26 July 2012; published 21 September 2012.

[1] An extensional earthquake sequence occurred in 2004–8 across a graben in the South Lunggar Rift on the Tibetan Plateau. We use InSAR data to determine the location, fault geometry and slip distribution of these earthquakes and to test whether the sequence is compatible with static stress triggering. The Mw 6.2 and 6.3 earthquakes in 2004 and 2005 both ruptured west-dipping faults on the east side of a graben. In 2008, a Mw 6.7 earthquake ruptured a pair of east-dipping fault segments on the other side of the graben, offset from the earlier ruptures. We compute first-order dislocation models of stress change and demonstrate that the order and spatial configuration of this sequence of events is compatible with triggering by static stress transfer. A continuation of the sequence would be most likely to occur on the northern extension of the 2008 rupture, although variable slip rate along the rift may mean that the sequence has run its course. The InSAR data for the 2008 earthquake also reveal slip on a fault that cuts the graben at a highly oblique angle. We suggest that this is a release fault accommodating differential throw in the hanging wall, and associate the deformation with a Mw 6.0 aftershock. Activity on such a release fault has not been directly imaged before. The Zhongba sequence is one of several examples of recent clustered normal-fault earthquakes on the Plateau, and may be an example of phase-locking of similar faults.

**Citation:** Ryder, I., R. Bürgmann, and E. Fielding (2012), Static stress interactions in extensional earthquake sequences: An example from the South Lunggar Rift, Tibet, *J. Geophys. Res.*, *117*, B09405, doi:10.1029/2012JB009365.

## 1. Introduction

[2] The Lhasa and Tethyan Himalayan terranes in the southern half of the Tibetan Plateau are dissected by a series of major NS-trending rift systems that accommodate east-west extension associated with the ongoing convergence of India and Asia [*Kapp et al.*, 2008; *Taylor and Yin*, 2009]. Many of the normal faults within these ~200 km-long rifts are active structures that rupture in small to moderate-sized earthquakes. In this paper we focus on the Zhongba earthquake sequence, which occurred between 2004 and 2008 within the South Lunggar Rift in the southwest part of the Plateau. The South Lunggar Rift (Figure 1a) consists of two basins on either side of the central Gangdese and South Lunggar Ranges, with active normal faults on either side of the high topography dipping into the basins, and further activity beyond the range-bounding faults. A hanging wall lake sits in the valley adjacent to the central part of the east-dipping bounding fault. In the southern part of this same valley, minor normal faults with less pronounced topography cut up the hanging wall of the range-bounding fault. There may also be active faulting in the northern part of the valley, though no obvious fault scarps are present. Extension rates across the southern part of the rift are estimated to be 1 mm/yr, increasing to 2.5 mm/yr in the northern part [*Styron et al.*, 2011]. Figure 1b is a topographic profile across the line A-A′ marked in Figure 1a. The scarps of several normal faults are clearly visible, including the ones that ruptured in the 2004 and 2008 earthquakes. The schematic in Figure 1c is a simplified interpretation of the sub-surface structure beneath the rift.

[3] The first two earthquakes of the Zhongba sequence (Mw 6.2 and 6.3) occurred in 2004 and 2005 and ruptured the eastern side of a graben within the rift. A Mw 6.7 earthquake in 2008 ruptured a pair of faults on the western side of the graben, offset from the earlier opposing ruptures. In addition, a Mw 6.0 aftershock occurred one month after the 2008 event, rupturing a transverse fault in the middle of the graben. Since these events were located in close spatial proximity, they offer a good opportunity to investigate static stress triggering between normal faults. Excellent InSAR images allow us to explore in detail the nature of these earthquakes and how one event might trigger another by static stress transfer. We start by presenting Envisat interferograms for the three main earthquakes, and inverting the line-of-sight displacements for distributed fault slip on each of the three main ruptures. We then show postseismic

[1]School of Environmental Sciences, University of Liverpool, Liverpool, UK.
[2]Berkeley Seismological Laboratory, University of California, Berkeley, California, USA.
[3]Jet Propulsion Laboratory, California Institute of Technology, Pasadena, California, USA.

Corresponding author: I. Ryder, School of Environmental Sciences, University of Liverpool, Liverpool L693GP, UK. (i.ryder@liv.ac.uk)

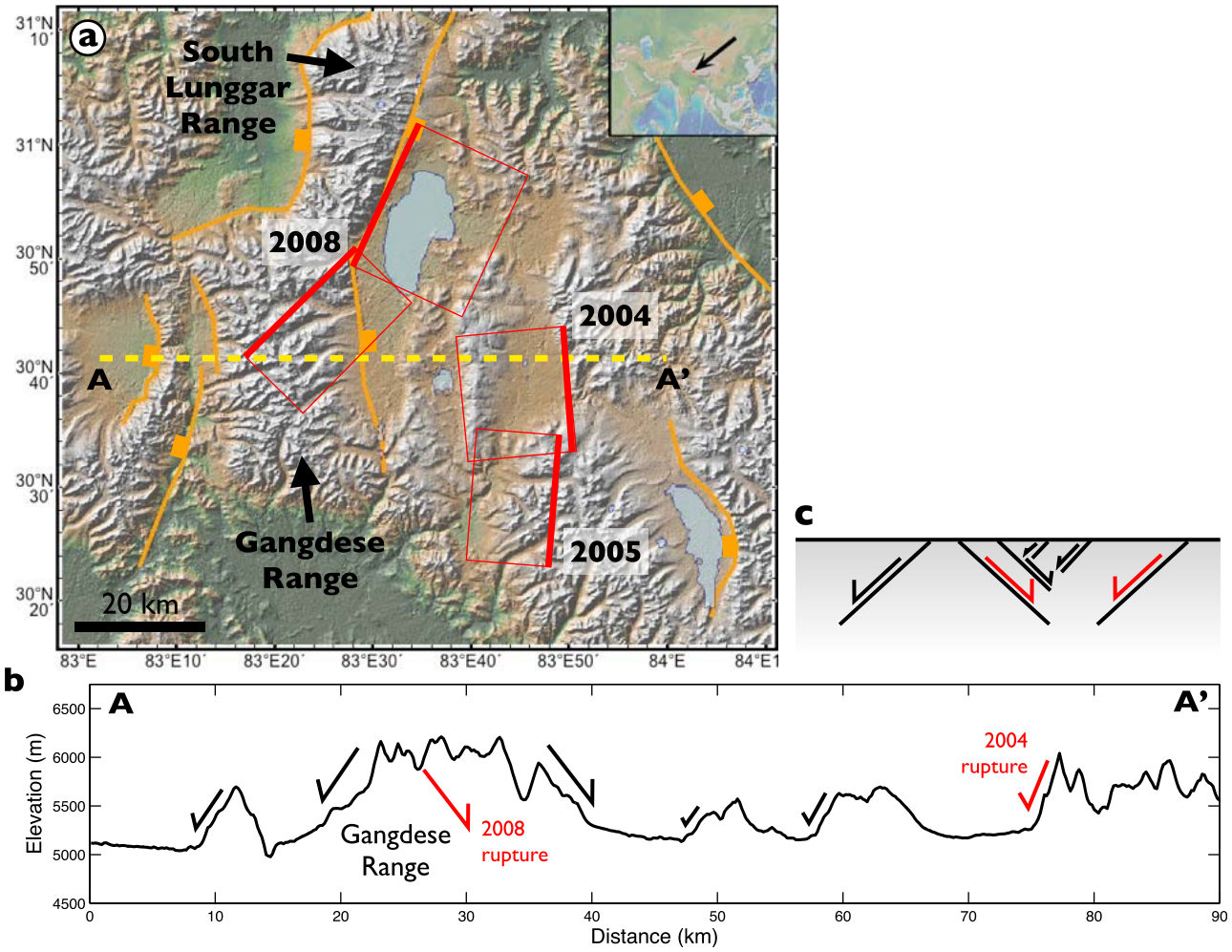


**Figure 1.** (a) Topographic map of the South Lunggar Rift, with location shown in inset. Orange lines mark faults as mapped by *Taylor and Yin* [2009]. Red boxes mark the surface projection of faults that ruptured during the Zhongba sequence, as modeled in the present study, with the thicker red line on each box representing the fault trace. Yellow dashed line marks location of profile in Figure 1b. (b) Topographic profile across the rift, along line A-A′. (c) Schematic cross section across the rift showing the spatial relationship between faults at depth.

interferograms for the 2008 event showing localized deformation across the transverse fault. The slip distributions for the three main shocks are used to compute how the stress on each of the faults evolves over the course of the sequence, and therefore to evaluate whether the timing and spatial configuration of the ruptures is consistent with static stress triggering. The geometry of the Zhongba system is generalized to highlight the key characteristics of static stress triggering for normal faulting earthquakes. Finally we place the Zhongba sequence in the context of other clusters of normal faulting earthquakes that have occurred on the Plateau and elsewhere, and discuss the implications of phase-locking in extensional systems.

## 2. The Zhongba Main Shocks

### 2.1. InSAR Data

[4] Envisat SAR acquisitions covering each of the three earthquakes were processed in pairs using the ROIPAC software [*Rosen et al.*, 2004]. All scenes were acquired in image mode 2 (IM2), for which the nominal look angle is 23°. A 90 m DEM produced from the Shuttle Radar Topography Mission (SRTM) was used to correct for topographic phase [*Farr et al.*, 2007], and the remaining phase was unwrapped using the branch cut algorithm of *Goldstein et al.* [1988]. Table 1 lists the SAR pairs used for each of fifteen interferograms presented in the main part of this paper and Figure 2 shows the time interval covered by each interferogram, relative to the earthquakes. In addition, a descending Envisat wide-swath interferogram is shown in Figure S1 of the auxiliary material.[1] Many other IM2 pairs were also processed, but had poor coherence, or the fringe pattern was heavily truncated at the edges of the scene. Of the selected interferograms, two each cover the 2004 and 2005 earthquakes (Figures 3 and 4, respectively), and four span the

[1]Auxiliary materials are available in the HTML. doi:10.1029/2012JB009365.

**Table 1.** Envisat Interferograms Shown and/or Used in the Analysis in This Paper[a]

| Number | Date 1 | Date 2 | Track | Frame(s) | $B_{perp}$ (m) | Desc/Asc |
|---|---|---|---|---|---|---|
| | | | *Earthquake 1: 11 July 2004* | | | |
| 1 | 040317 | 040908 | 119 | 2979, 2997 | 80 | Desc |
| 2 | 040421 | 041013 | 119 | 2979, 2997 | 181 | Desc |
| | | | *Earthquake 2: 7 April 2005* | | | |
| 3 | 041031 | 050703 | 384 | 603 | 124 | Asc |
| 4 | 050302 | 050615 | 119 | 2997 | 50 | Desc |
| | | | *Earthquake 3: 25 August 2008* | | | |
| 5 | 061210 | 081109 | 384 | 603, 621 | 110 | Asc |
| 6 | 070430 | 081110 | 391 | 2979, 2997 | 59 | Desc |
| 7 | 070430 | 081006 | 391 | 2979, 2997 | 78 | Desc |
| 8 | 071107 | 081022 | 119 | 2979, 2997 | 28 | Desc |
| | | | *2004 and 2005 Earthquakes* | | | |
| 9 | 040317 | 050511 | 119 | 2979, 2997 | 37 | Desc |
| | | | *2008 (Postseismic)* | | | |
| 10 | 080917 | 090415 | 119 | 2979, 2997 | 17 | Desc |
| 11 | 081005 | 081214 | 384 | 603, 621 | 70 | Asc |
| 12 | 081006 | 081110 | 391 | 2979 | 22 | Desc |
| 13 | 081006 | 081215 | 391 | 2979 | 81 | Desc |
| 14 | 081022 | 081231 | 119 | 2979, 2997 | 69 | Desc |
| 15 | 081110 | 090504 | 391 | 2979 | 51 | Desc |

[a]Numbers in first column correspond to the labels in Figures 3–6 and Figure 11. Dates in second column are in yymmdd format. Final column denotes whether the satellite track is descending (north to south) or ascending (south to north).

2008 earthquake (Figure 5). In addition, interferogram 9 covers both the 2004 and 2005 events, and the composite image in Figure 6 shows the spatial relationship of the ruptures and the deformation patterns across the graben. Except for the 2004 event, there are both ascending and descending interferograms. As can be seen from Figures 3–6, coherence in the interferograms collectively is moderate to good. The 2008 IM2 interferograms (Figure 5) show marked incoherence in the ice-covered footwall, while the wide-swath interferogram in Figure S1 of the auxiliary material displays better footwall coherence. In all interferograms, the hanging wall lake is incoherent.

### 2.2. Patterns of Static Ground Displacement

[5] In general, normal fault ruptures are characterized by footwall uplift and hanging wall subsidence, with the subsidence being several times greater than the uplift. In addition, horizontal displacement vectors are smaller than the maximum vertical subsidence. These characteristics, together with the sensitivity of Envisat IM2 to vertical displacements, means that we should expect a proliferation of line-of-sight displacement fringes in the hanging walls of normal fault ruptures, relative to the footwalls. Furthermore, we can expect a steeper gradient of fringes near the fault trace than on the far-field side of the hanging wall basin. Interferogram 1 clearly shows a densely spaced, asymmetric set of fringes on the left of the image, flanked by less than one fringe on the right of the image. From this it can be inferred that the 2004 earthquake ruptured a west-dipping fault, with the fault trace marked by the black arrows. By similar reasoning applied to interferogram 4, we infer that the 2005 earthquake also ruptured a west-dipping fault. Although all of the 2008 interferograms are incoherent over the mountain ranges in the center of the rift, it is clear from the asymmetry of the fringe pattern as well as the geomorphology (the mountain range and the lake) that the 2008 event ruptured an east-dipping fault. Thus, in a broad sense this data set shows extension across a graben within the rift zone, although as can be seen from the composite image in Figure 7 (middle), the east- and west-dipping ruptures are offset from each other in a N-S direction. The greater number of fringes in the 2005 image compared to the 2004 image implies that the second earthquake was larger than the first (assuming the ruptures were at the same depth), which agrees with the GCMT moment magnitudes of 6.2 (2004) and 6.3 (2005). The density of fringes for 2008 is similar to that for 2005, but the areal extent of fringes is greater than for the previous two earthquakes

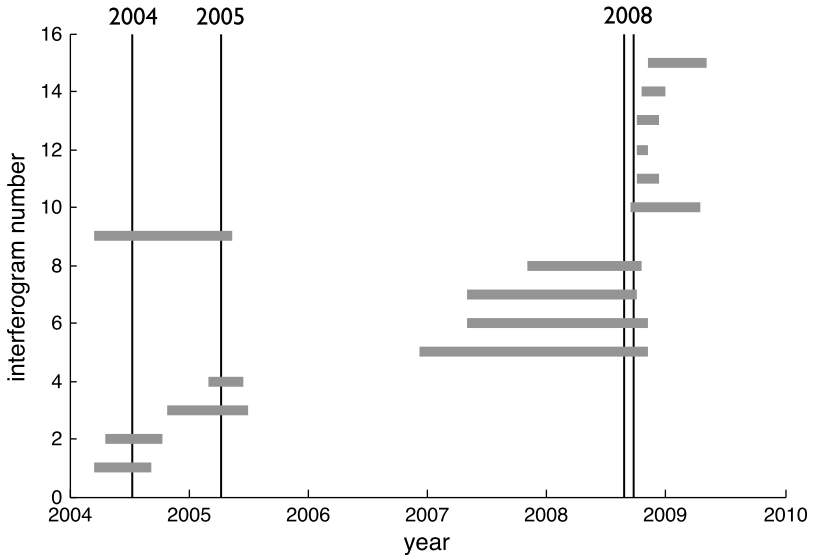


**Figure 2.** Time intervals covered by each of the interferograms shown in Figures 3–6 and Figure 11. Interferogram numbers correspond to those in the figures. Grey bars show time intervals and black vertical lines mark the times of the 2004, 2005 and 2008 earthquakes plus the 2008 aftershock.

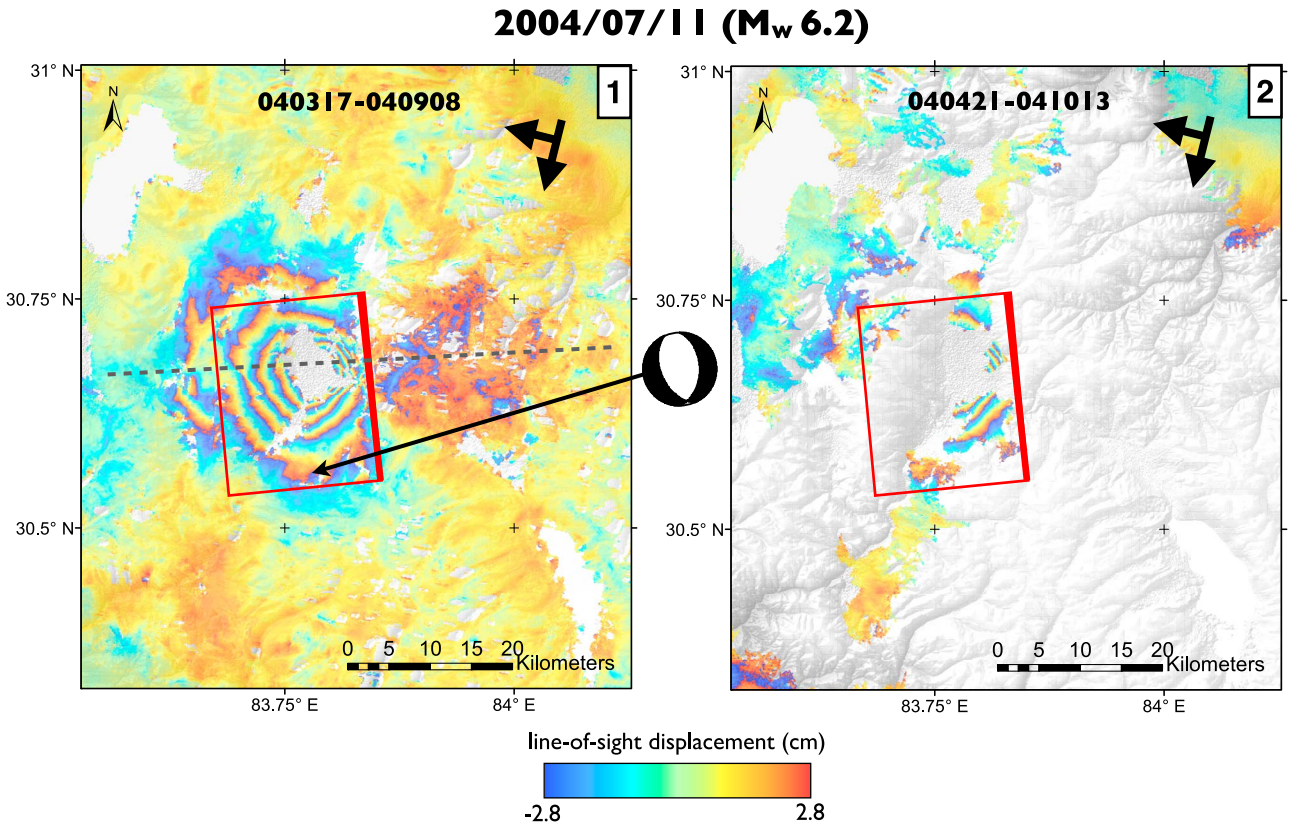


**Figure 3.** Wrapped coseismic interferograms for the 2004 Zhongba earthquake. Start and end dates are given in yymmdd format at the top of each image, and numbers in the top right of each image correspond to those in Table 1. The focal mechanism between the images is from the Global CMT catalog, and the arrow points to the GCMT location. Red box represents surface projection of modeled fault. Grey dashed line on interferogram 1 marks location of the top profile in Figure 7.

combined. This is consistent with the significantly larger moment magnitude (6.7) of the 2008 earthquake. The GCMT focal mechanisms for all three earthquakes (Figures 3–5) are consistent with the inferences of fault geometry and rupture type made from the InSAR data, although we note that the strike of the nodal planes in the 2005 focal mechanism are slightly rotated with respect to the InSAR-inferred fault trace. The GCMT solutions locate the earthquake centroids between 12 and 30 km south of the center of the fringe patterns, consistent with the finding by *Elliott et al.* [2010] of a 15–30 km SSE-ward bias of GCMT locations throughout Tibet. Profiles of line-of-sight displacement for the three large earthquakes are shown in Figure 7, with the displacements being displayed up-side-down to give a sense of the differential vertical motion across the faults. In all three profiles, a clear range increase is observed on one side of the fault, and a range decrease several times smaller on the other side.

### 2.3. Inversion for Slip Distribution

[6] The three sets of coseismic interferograms are used to estimate slip distributions on dipping normal faults. The interferograms are down-sampled and inverted for slip on a discretized fault plane or planes, following the procedure described by *Ryder et al.* [2010] in their analysis of the 2008 Nima-Gaize earthquake. For each event, the strike, length and location of the fault trace are well-constrained by the InSAR deformation field. The dip and rake are initially constrained by considering the GCMT nodal plane that is consistent with the InSAR fringe pattern, and are subsequently adjusted by small increments to reduce the residuals. For the 2004 and 2005 events, a single fault plane is specified, while for the 2008 event, a two-fault model is implemented to reflect the curvature of the fringe pattern away from the basin and into the range itself.

[7] Fault parameters are listed in Table 2, and the slip distributions for the three earthquakes are shown together in Figure 8. All three ruptures are buried, with only a small amount of slip occurring in the top few kilometers. This is a persistent characteristic of extensional ruptures [*Cinti et al.*, 1999; *Mariucci et al.*, 2010; *Pondrelli et al.*, 2010; *Ryder et al.*, 2010, 2012]. Field investigation in the area of the 2008 northern rupture did not bring to light any surface rupture (Mike Taylor, pers. comm.), which is supported by our inference of buried slip. The slip is dominantly dip slip, with a small amount of sinistral slip. The 2004 event had a maximum slip of 0.51 m at a depth of 8–10 km, and the 2005 event had a maximum slip of 0.93 m, also at a depth of 8–10 km. The 2008 event had three local slip maxima, one of 1.02 m at a depth of 10–12 km on the northern fault segment, and two of 1.34 m and 0.97 m at a depth of 8–10 km on the southern segment. While the northern 2008 segment co-

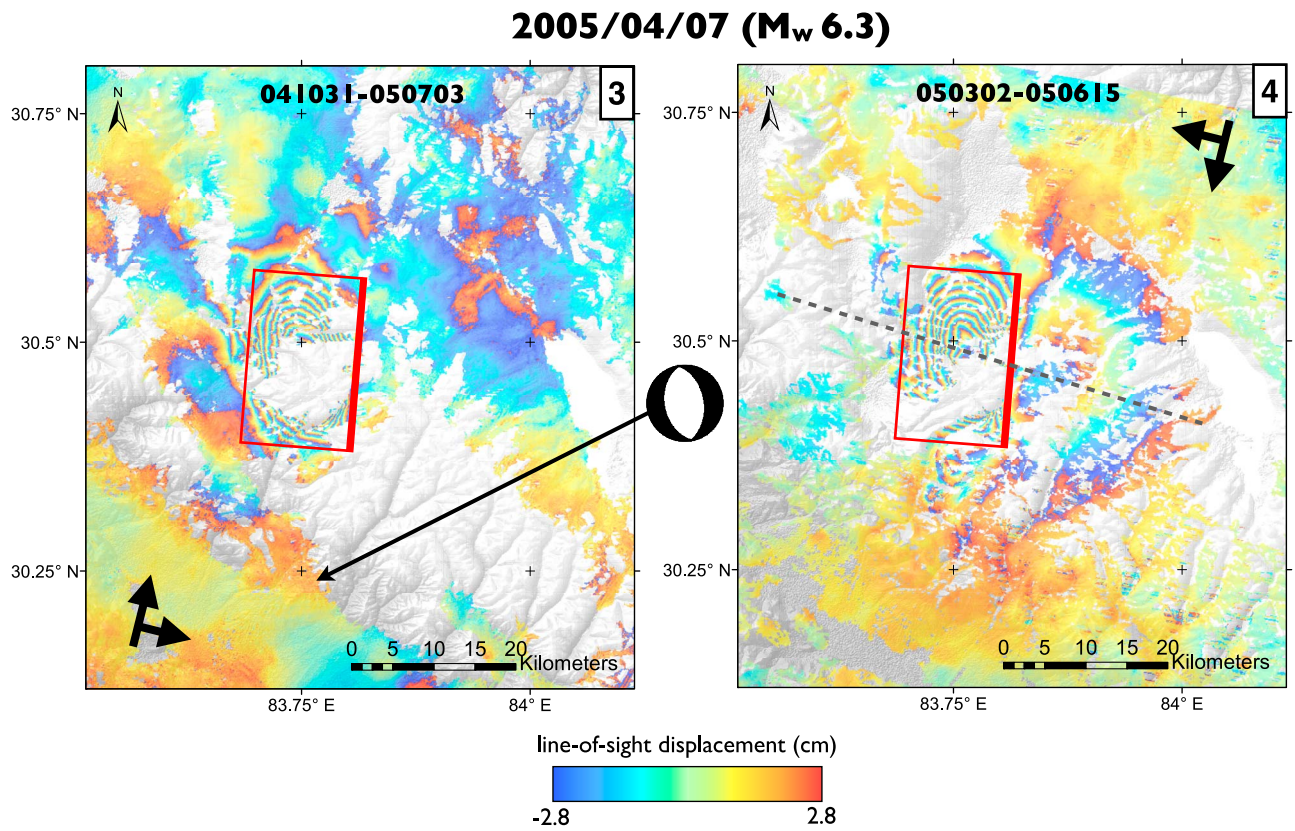


**Figure 4.** Wrapped coseismic interferograms for the 2005 Zhongba earthquake. Start and end dates are given in yymmdd format at the top of each image, and numbers in the top right of each image correspond to those in Table 1. The focal mechanism between the images is from the Global CMT catalog, and the arrow points to the GCMT location. Red box represents surface projection of modeled fault. Grey dashed line on interferogram 4 marks location of the middle profile in Figure 7.

locates with the range-bounding fault to the west of the lake (see Figure 1), the southern segment cuts through the range, i.e., the southern part of the range-bounding fault does not appear to have ruptured. Although unwrapping errors in the wide-swath interferogram made it unsuitable for inclusion in the 2008 slip inversion, we used the slip distribution derived in the IM2 inversion to run a forward model for comparison with the wide-swath image. The interferogram and forward model are shown in Figure S1 of the auxiliary material, along with the residual. The residuals everywhere are less than $\sim$ 4 cm, and further support the inference of the second 2008 event having ruptured a fault that cuts through the range, rather than the range-bounding fault. We also carried out inversions where the trace of the southern fault is coincident with the range front, but the resulting models have very large residuals in the southern part (Figure S2 of the auxiliary material), and so a range-front rupture can be ruled out. We note that the 2005 event also ruptured through an area of high topography, rather than being associated with a geomorphically expressed fault. The InSAR-derived slip distributions have equivalent moment magnitudes of 6.3, 6.3 and 6.7 for the three events, compared with the GCMT magnitudes of 6.2, 6.3 and 6.7. The interferograms are displayed in their unwrapped form in Figures 9 and 10, along with forward-modeled line-of-sight displacements and residual fields. A pronounced residual appears in all of the 2008 images (gray circles in Figure 10), which we interpret as deformation associated with the September aftershock, discussed below. The InSAR-derived slip models from the study of the Zhongba earthquakes by *Elliott et al.* [2010] study are comparable with the results of the present study, with small variations in strike and dip of the fault planes.

## 3. Aftershock Deformation

[8] Six postseismic interferograms for the 2008 earthquake (Table 1 and Figure 11) all reveal deformation across a structure in the hanging wall basin, essentially perpendicular to the strike of the range front. Since the first postseismic interferogram (no. 10) brackets a Mw 6.0 aftershock on 25 September 2008, we infer that deformation initiated on this structure during the aftershock, and subsequently continued aseismically in the form of afterslip. The aftershock line-of-sight displacement profile across the structure in Figure 12b (again, displayed up-side-down) shows large positive range change on the NE side, with a smaller negative lobe on the SW side. Such a pattern is not dissimilar to the main shock profiles in Figure 7 and, notwithstanding the contribution of horizontal as well as vertical to the line-of-sight displacements, suggests a component of normal motion. Included in Figure 12 is a schematic diagram showing the relationship between the main 2008 fault and the

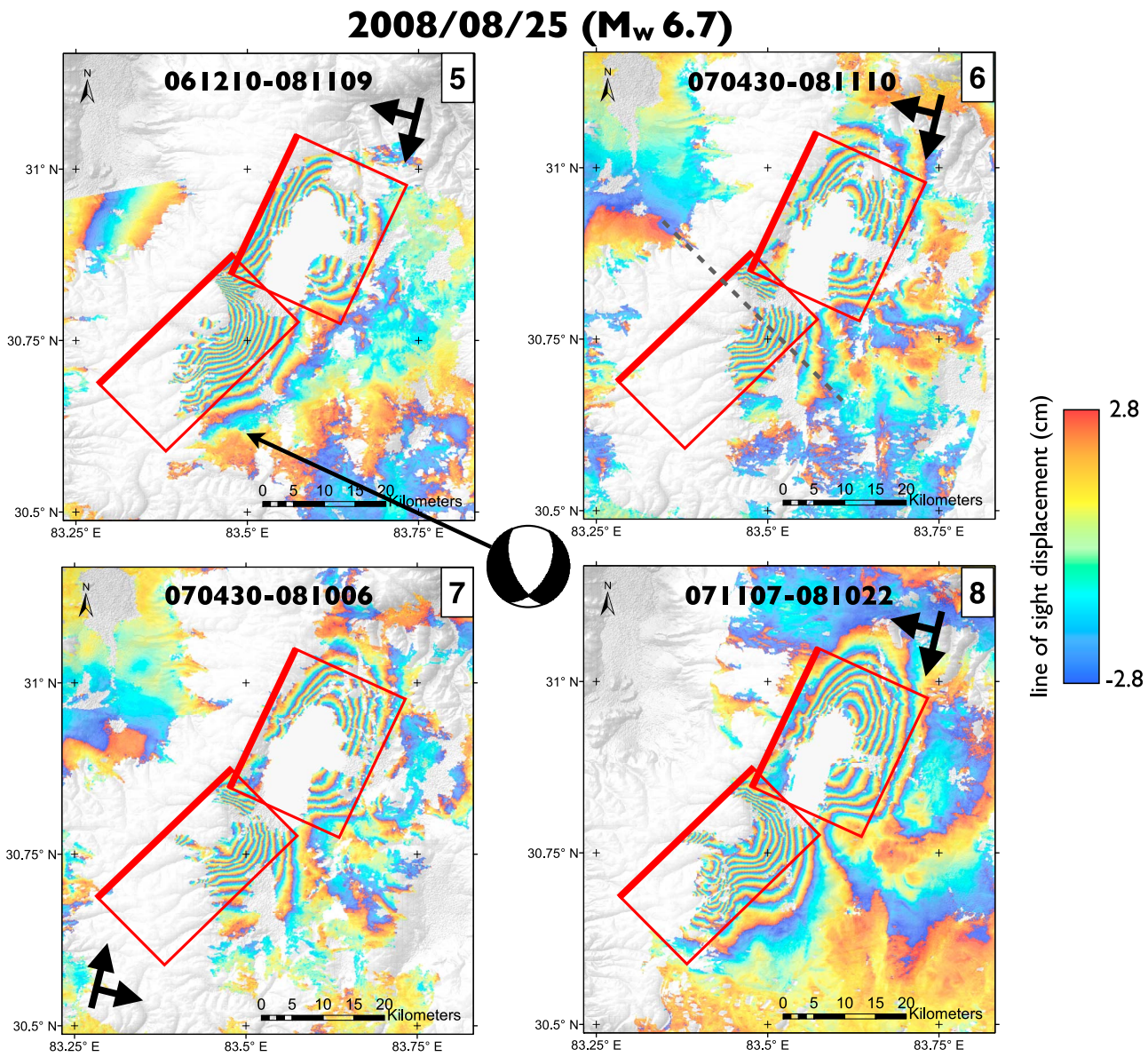


**Figure 5.** Wrapped coseismic interferograms for the 2008 Zhongba earthquake. Start and end dates are given in yymmdd format at the top of each image, and numbers in the top right of each image correspond to those in Table 1. The focal mechanism in the center is from the Global CMT catalog, and the arrow points to the GCMT location. Red box represents surface projection of modeled fault. Grey dashed line on interferogram 6 marks location of the lower profile in Figure 7.

transverse fault. The GCMT focal mechanism for the aftershock puts the strike of nodal plane 2 at 302°, consistent with the structure in the interferogram. The dip of the nodal plane is 77° and the rake is −165°, corroborating the inference of normal motion made from the InSAR data. The range-orthogonal orientation of the structure and the normal component of slip is strongly suggestive of this structure being a release fault as described by *Destro* [1995], that is, a structure in the hanging wall of a normal fault that accommodates differential subsidence. Active slip on such structures has not been observed before, only inferred from structural relationships in the field or from seismic sections. We note that release faults are distinct from the commonly recognized transfer faults, which accommodate deformation in between two en echelon faults or fault segments.

[9] To interpret the aftershock deformation seen in the interferogram, we run simple forward models using the fault parameters of the nodal plane referred to above and uniform slip on a single rectangular dislocation plane. We choose not to invert the line-of-sight displacements formally, because (i) only one interferogram covers the aftershock, and the deformation pattern is truncated by the hanging wall lake; (ii) since the line-of-sight displacements associated with this Mw 6 event are only several times greater than the level of noise in the interferogram, artifacts may be introduced into an inverted slip model; and (iii) there is some uncertainty about

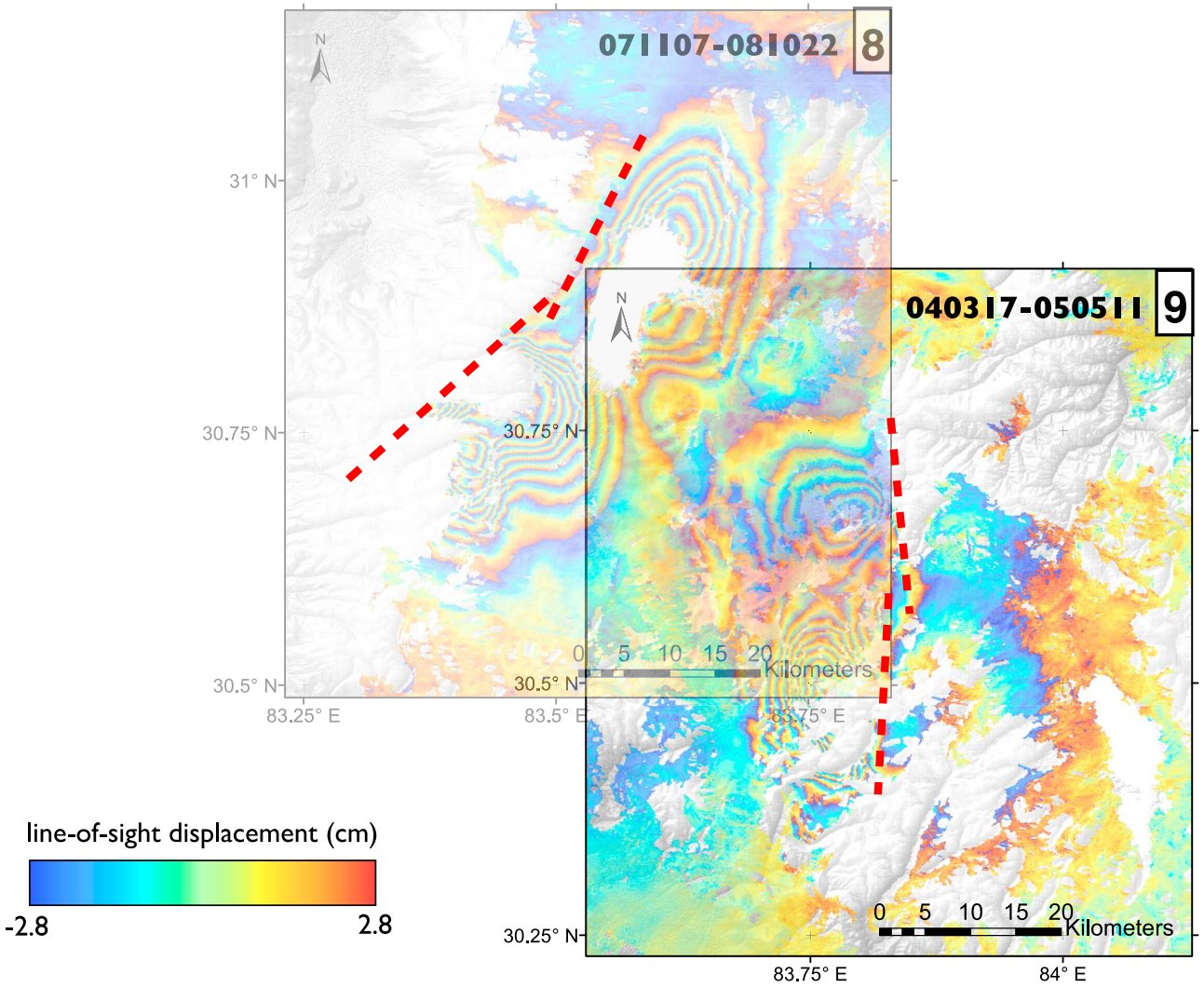


**Figure 6.** Composite of two interferograms: no. 8 (shown in Figure 4) spans the 2008 event, and no. 9 spans both the 2004 and 2005 events. The two images are aligned so as to show the spatial relationship between the fringe patterns for each earthquake. Red dashed lines denote traces of faults inferred in this study.

whether the negative (blue) lobe to the east of the positive (red) lobe in interferogram 10 is real or not. The key objective of forward modeling is to test whether the observed line-of-sight deformation is consistent with the transtensional GCMT mechanism. The fault length is estimated from the interferogram to be 13 km. The displacement profile in Figure 12 does not show a discontinuity, implying that the fault does not break the surface, so the top depth is set to be 2 km, similar to the upper depth of slip obtained in the main shock inversions. The lower depth of 8 km is chosen so as to make the widths of the lobes match those in the interferogram. Slip is assumed to be uniform across the fault plane. The modeled displacements are converted to Envisat descending line-of-sight displacements for comparison with interferogram 10. Two model outputs are shown in Figures 12c and 12d, for rakes of −165° and −135° respectively. The GCMT rake (−165°) gives an asymmetrical quadrant pattern, as seen in the aftershock interferogram (no. 10). The alternative rake gives a simple asymmetrical two-lobe pattern, as seen in the postseismic interferograms (nos. 11–15). The likelihood of one rake over the other is discussed in Section 6.2.

## 4. Stress Evolution Across the Graben

### 4.1. The Three Main Shocks

[10] To test whether later earthquakes in the Zhongba sequence may have been triggered by earlier ones, we run models to compute the progression of Coulomb stress changes on the normal faults on either side of the graben. First, the stress changes on all the faults due to slip in the 2004 rupture are computed (Figure 13, stage 1), and then stress changes after the 2005 rupture (stage 2) due to both earthquakes combined are calculated. We are primarily interested in whether stress changes on any or all of each fault, at successive stages of the sequence, exceed the commonly accepted triggering threshold of ~0.1 bars [e.g., *King et al.*, 1994; *Lin and Stein*, 2004]. We note that of the two fault segments that ruptured in the 2008 earthquake, the

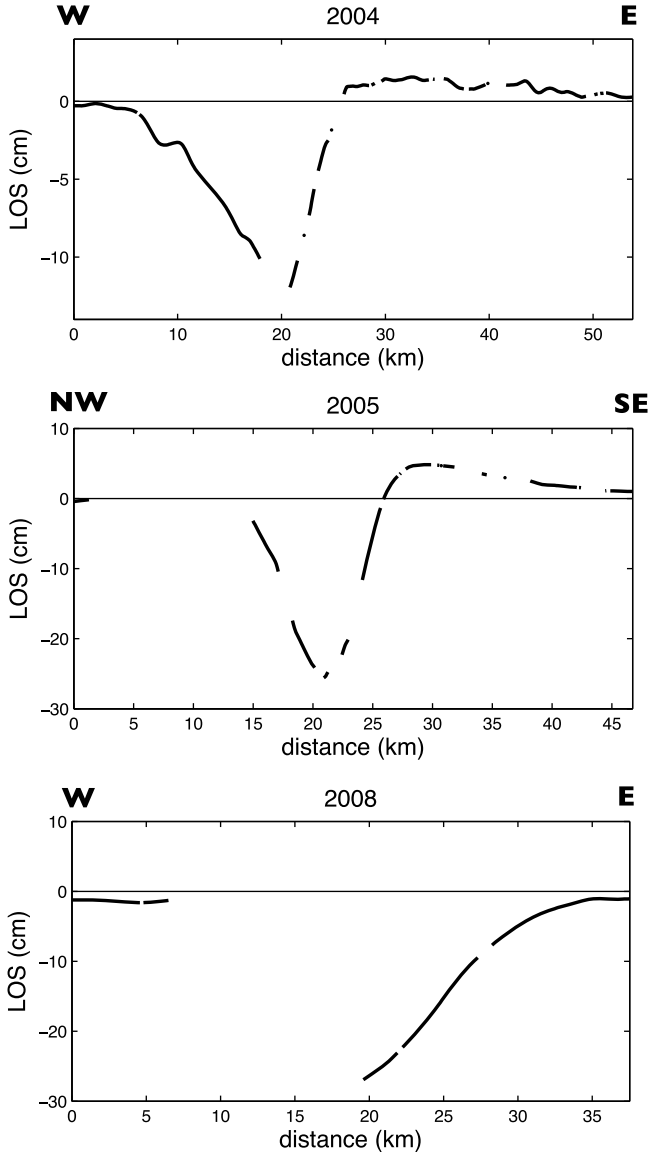


**Figure 7.** Line-of-sight (LOS) displacement profiles across interferograms 1, 4 and 6. Profile locations are marked by gray dashed lines on these interferograms in Figures 3–5. The line-of-sight displacements are displayed with positive and negative reversed relative to the interferogram images, in order to give a sense of vertical displacement.

northern one is inferred from seismological data to have ruptured first [*Elliott et al.*, 2010], and so we consider the relative stress changes on the northern and southern segments at stage 2. Stress drops on the faults where slip occurred are also of interest. Note that all stress calculations are carried out for the fault patches shown in stage 0 of Figure 13. All fault patches are approximately 2 km × 2 km, and so actual stress changes over smaller areas may be greater than calculated. We do not overly concern ourselves here with the static stress changes imposed by the first 2008 sub-rupture (stage 3) on the second (stage 4), since dynamic stresses may have played an important role, and there is no way of distinguishing between static and dynamic effects. For all model runs, Coulomb stress changes are computed on each fault patch using the rake value estimated in the distributed slip inversions, and an effective friction coefficient of 0.4, as is commonly used in stress interaction studies [*Freed*, 2005].

[11] We find that in stage 1 (2004 event), the maximum stress drop on the ruptured fault is 25 bars, while Coulomb stress changes on the 2005 fault are positive over most of the plane, reaching a maximum of 1 bar on the northern side and decreasing to 0.25 bars on the southern side. Stress changes on the northern 2008 segment are positive everywhere, but much smaller (≤0.1 bar) than on the 2005 fault. The southern 2008 segment experiences mostly negative stress changes of ∼0.1 bar, with a small area of minor positive stress change on the northernmost tip. In summary, the 2004 earthquake brings the 2005 fault closer to failure well above the triggering threshold, but not the 2008 fault. In stage 2 (2005 event), the maximum stress drop on the fault that slipped is 55 bars, and the effect of the new rupture is essentially to enhance the previous stress changes on the 2008 segments: the positive stress changes on the northern segment are now increased up to ∼0.2 bars, while the negative stress changes on the southern segment are ∼0.2 bars. The maximum stress drop in the 2008 earthquake (stages 3 and 4) is 80 bars. To test whether the range-oblique fault was favored over the range-bounding fault in terms of stress change, calculations of total stress change were also carried out for a fault bounding the eastern side of the Gangdese Range. The result is a little inconclusive, in that while the positive stress change at the northern end of the bounding fault is several times greater than for the oblique fault, the negative stress change is also several times greater. We also note that due to the closeness in time of the two 2008 sub-ruptures, dynamic stressing from the northern rupture may have played a role in determining which southern fault failed.

[12] Overall, the Zhongba sequence is consistent with the idea of earthquakes being triggered by static stress changes from previous nearby earthquakes. The 2004 earthquake increased stress on the segment along strike to the south, which ruptured in 2005. The 2004 and 2005 events collectively caused a stress increase on the northern fault across the graben, and a stress decrease on most of the southern fault. After three years, the northern segment ruptured first. Calculations of the sort carried out here can only support the hypothesis of static stress triggering, and do not constitute a proof that triggering occurred. The best we can do is to accumulate evidence for or against the proposed mechanism.

### 4.2. The Hanging Wall Release Fault

[13] To explore further evidence for stress interaction, we investigate the hanging wall release fault. The objective is to test whether a range-orthogonal fault in the 2008 hanging wall basin is consistent with stress changes resulting from

**Table 2.** Fault Parameters for the Slip Models Shown in Figure 8[a]

| | Longitude (°) | Latitude (°) | Strike (°) | Dip (°) |
|---|---|---|---|---|
| 2004 | 83.834 | 30.653 | 175 | 45 |
| 2005 | 83.808 | 30.482 | 183 | 44 |
| 2008 (N) | 83.547 | 30.950 | 25 | 40 |
| 2008 (S) | 83.392 | 30.780 | 45 | 50 |

[a]Rake is allowed to vary.

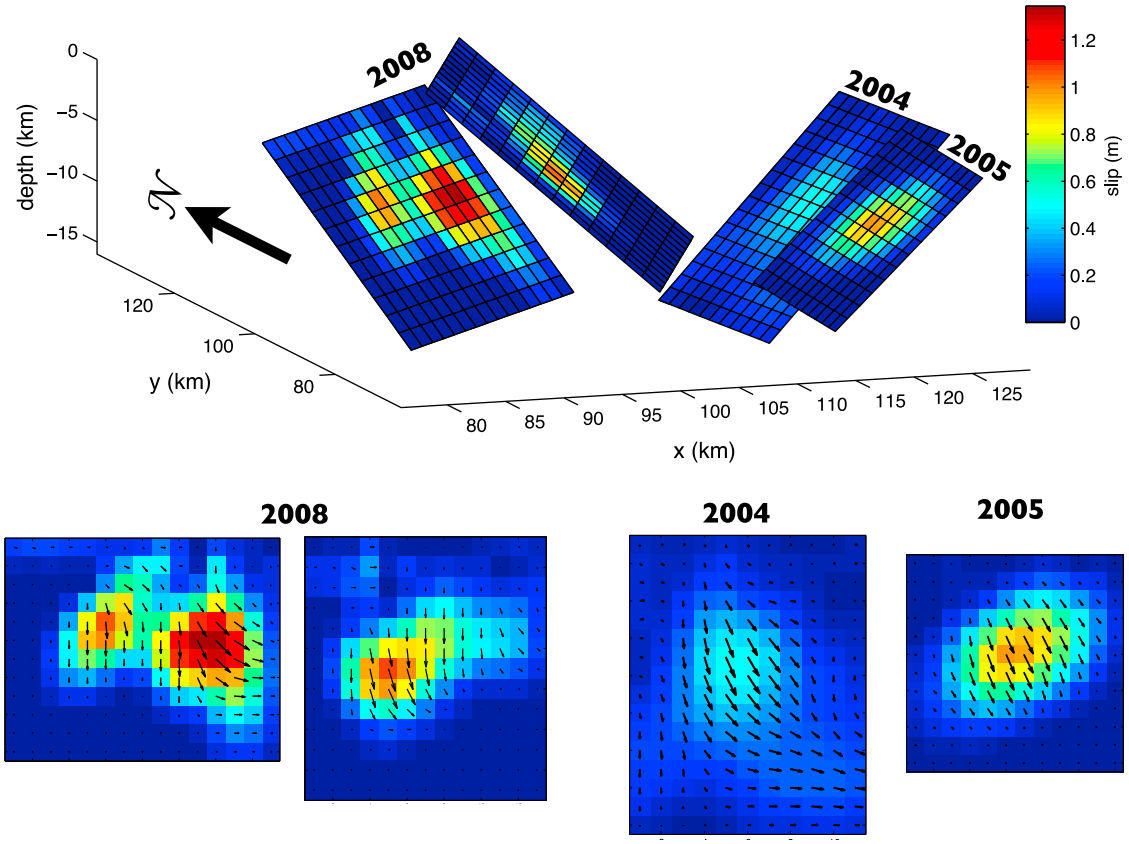


**Figure 8.** Slip distributions on the three Zhongba main shock faults, as obtained in the InSAR inversions. Black arrows in the lower panels show the slip vector on each individual fault patch.

the main shock sequence. Coulomb stresses from the three Zhongba main shocks are computed at 5 km depth and resolved onto the geometry of the release fault, assuming a rake of −165° (Figure 14). While much of the area around the main shock faults is in a stress shadow, there is a zone of positive stress change of ∼2 bars exactly where the aftershock occurred. A similar situation obtains if the rake is varied to −135°. Thus, the mechanics of release faulting, as seen here for the first time, also appears to conform to the theory of triggering by static stress transfer.

## 5. Generalized Triggering Scenarios for Normal Faults

[14] *Nostro et al.* [1997] investigated static stress triggering of normal faults with particular reference to the 1980 Irpinia earthquake in Italy, which consisted of four subruptures. Even though these sub-events all occurred within 40 s of each other, the paper focuses on static stress changes, which are shown to explain the rupture sequence, rather than dynamic stressing. Following on from the analysis of *Nostro et al.* [1997], we now generalize the models described in Section 4.1 and summarize possible triggering scenarios that may occur in settings with multiple moderate-sized faults in close proximity. The generalized model consists of several faults oriented parallel to each other (we choose to align them N-S) and dipping in different directions, as are frequently found in zones of extension. One fault is referred to as the "master fault." Either side of the master fault are two faults dipping opposite ways, creating both a graben and a horst structure. This three-fault pattern is repeated alongstrike from the first set of faults. By imposing slip on the master fault, stress changes on terminal faults and on flanking synthetic and antithetic faults are evaluated, as well as stress changes on diagonally opposite faults. Note that the Zhongba sequence involved ruptures across a graben (with a horst nearby) and also on diagonally opposite faults (see Figure 1 and the composite interferogram in Figure 6). The spacing of the faults in the idealized model is chosen to be representative of the fault spacing in the Zhongba area. For the results shown in the Figure 15, all faults dip at 50° and extend from the surface down to a depth of 15 km. Stress changes are computed at a depth of 7.5 km. We are not concerned here with cross faults, only rift-parallel structures, and updip/downdip segmentation is not considered.

[15] Figure 15 shows the results of these calculations. In Figure 15a, Coulomb stresses imposed by the master fault are resolved onto antithetic structures, while in Figure 15b, stresses are resolved onto similarly dipping structures. The lobe patterns in each case are very similar. On either side of the master fault is a broad lobe of stress shadow extending well beyond the flanking faults, where earthquakes are unlikely to be triggered. However, a suite of calculations exploring model space indicates that a zone of positive range change may occur in the hanging wall in the top few kilometers of crust, where earthquakes may be triggered.

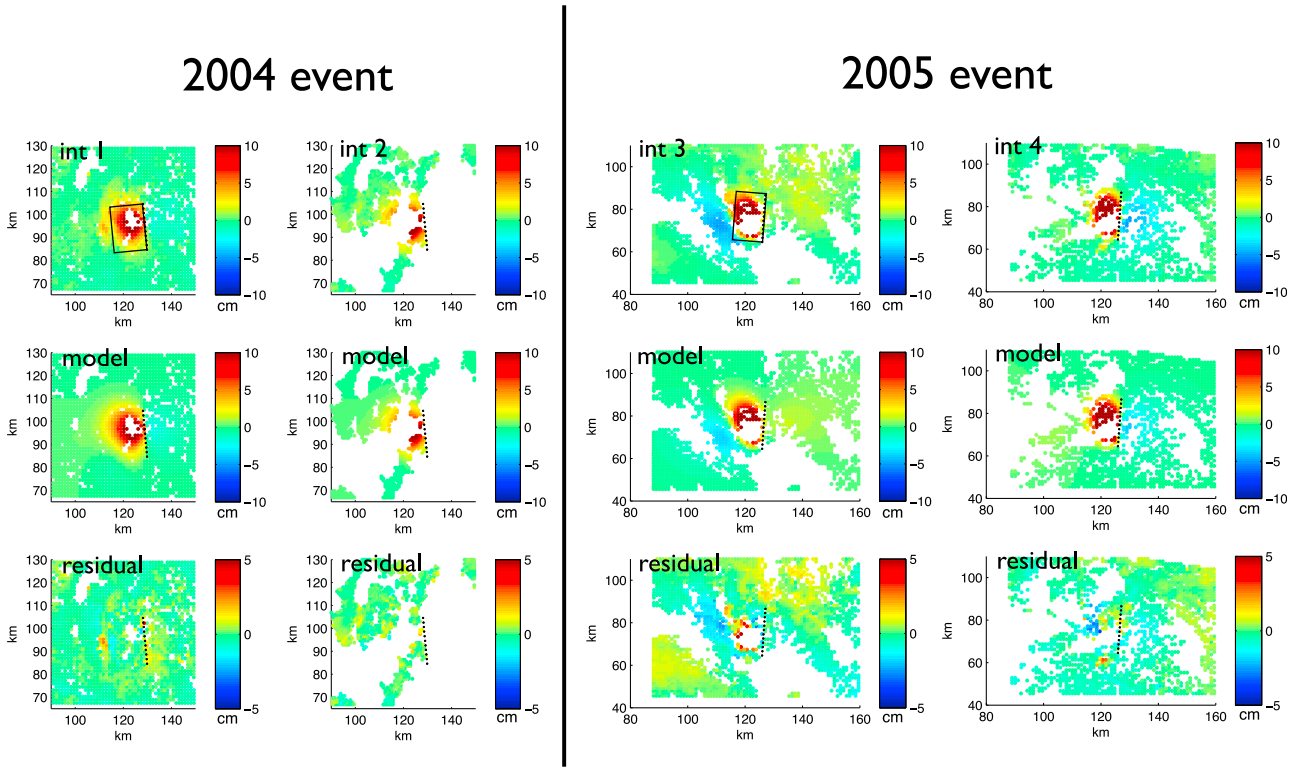


**Figure 9.** Unwrapped interferograms, forward models and residuals for the 2004 and 2005 earthquakes. Black dotted lines mark the fault trace and black box in upper left figure of each set shows the projection of the fault plane to the surface.

Whether or not this positive zone is present depends on the fault dip and how deeply buried the slip is. An example of shallow positive stress change in the hanging wall is shown in Figure 15. At either end of the master fault is a lobe of positive stress change, where faults are encouraged toward failure. In this example, diagonally opposite faults lie partially in the negative lobe and partially in the positive arc. If the along-strike spacing were greater, then such faults may lie wholly in the positive zone. Thus, diagonally opposite faults may be encouraged toward failure if they are sufficiently offset from the master fault. The Zhongba sequence conforms to the above in that (i) the 2004 earthquake triggered the 2005 earthquake along strike, not at its flanks; and (ii) the combined positive arcs from the 2004 and 2005 events brought a diagonally opposite fault closer to failure, and this fault ruptured in 2008. We note that the southern 2008 sub-rupture lies within the stress shadow of the 2004 earthquake, but it also lies within the terminal positive lobe of the first 2008 sub-rupture. Furthermore, the 2008 dual rupture may have involved dynamic effects from passing seismic waves, overriding any static stress changes. In general, however, the patterns of stress change outlined above have implications for the timing of ruptures within a rift system. For instance, if we say that the Zhongba sequence ruptured faults A, B, C and D in that order, we suggest that a sequence in the order A, D, C and B would not have occurred, since in this case fault D would at the time of failure have been solely in the stress shadow of the rupture on A.

## 6. Discussion

### 6.1. Recent Stress Changes in the Zhongba Area

[16] If, as the analysis in this paper suggests, the Zhongba sequence unfolded in the way it did as a result of static stress transfer, then it is natural to ask which faults are now "lit up." The stressing patterns summarized above would suggest that the most positively stressed areas are the ends of ruptures which are not in the flanks of other ruptures - in other words, immediately north of the 2008 rupture and immediately south of the 2005 rupture. The southern end of the 2005 rupture is very close to the edge of the South Lunggar Rift, but the range-bounding fault that ruptured in 2008 continues to the north for another 25 km. Figure 16 shows the results of modeling stress changes explicitly for the Zhongba fault system. Coulomb stress changes are computed on a horizontal section at 7.5 km depth, for a pure normal receiver fault striking at 30° and dipping at 45°. The stress change at the northern end of the 2008 rupture is over 1 bar. It is not possible to say for definite that the adjacent segment will fail, nor when (if it does). If all faults in this region are near the end of their earthquake cycle, we suggest that this northern segment would be the most likely of the mapped faults to host the next earthquake. However, as

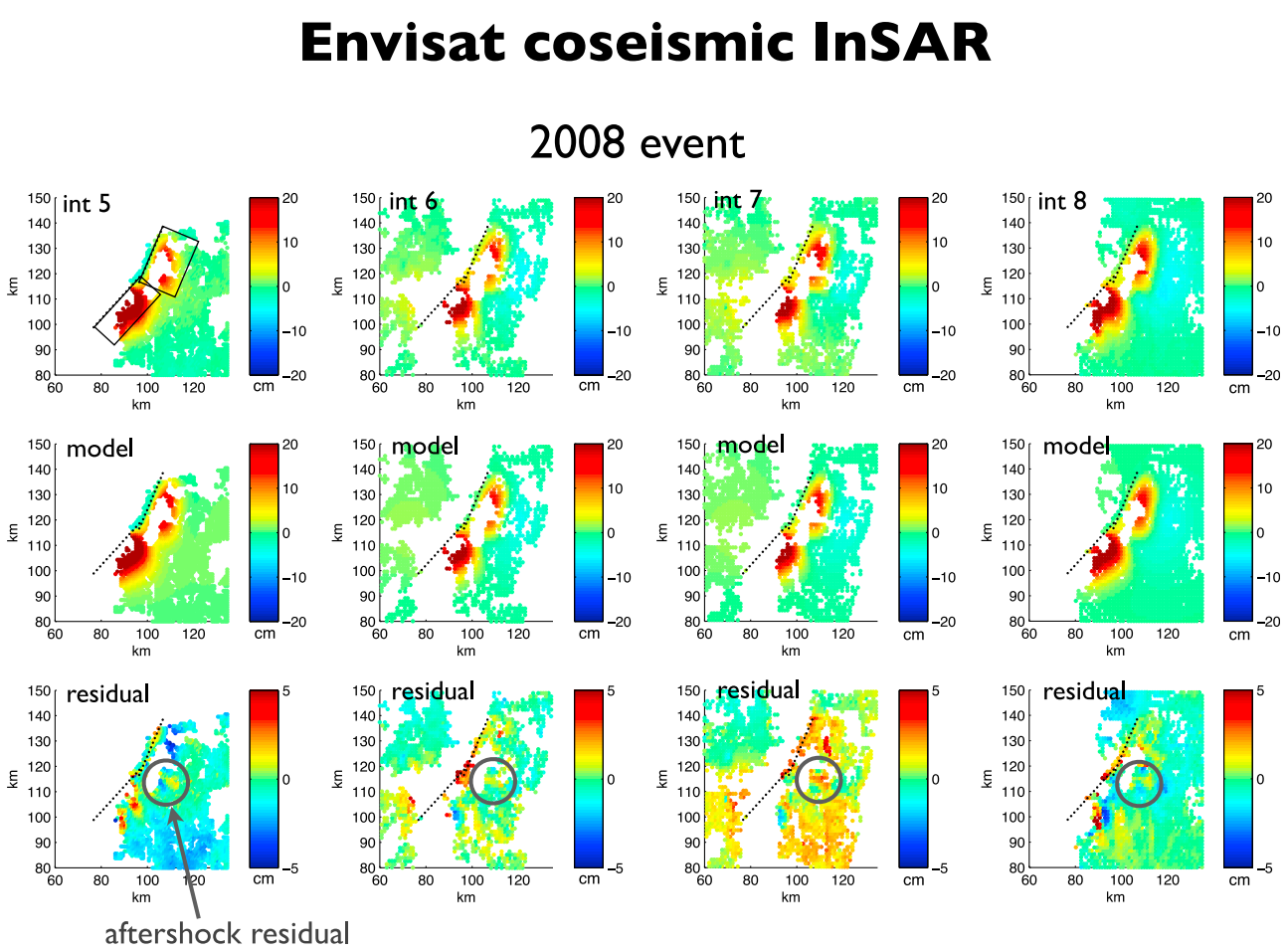


**Figure 10.** Unwrapped interferograms, forward models and residuals for the 2008 earthquake. Black dotted lines mark the fault traces and black boxes in upper left figure show the projection of the fault planes to the surface. Circles in lower panels indicate areas of significant residual due to an aftershock on 25 September 2008.

discussed in Section 6.5, slip rate variations along the rift may mean that all faults are not near the end of their cycle.

### 6.2. Mechanics of Release Faulting

[17] In this study we provide the first image of active deformation on a release fault. This type of fault was first recognized by *Destro* [1995] in his study of the Sergipe-Alagoas Basin, NE Brazil. Release faults develop in the hanging wall of normal faults in response to the bending associated with earthquake subsidence, which is variable along the length of the fault. The release faults are oblique to the main normal fault, and are sometimes perpendicular to it. Since the bending creates extension of layers in the hanging wall, release faults tend to have a strong component of normal motion parallel to the main fault. There may also be some strike-slip motion, since variable displacement on a dipping main structure will result in oblique shearing. Depending on which half of the main fault the release fault develops in, strike-slip motion may be dextral or sinistral.

[18] As described in Section 3, the localized hanging wall deformation we observe in the 2008 Zhongba data set can be modeled by oblique normal offset on a NE-dipping structure. The consistent feature seen in the aftershock interferogram and all the descending post-aftershock interferograms is a positive-negative lobe couplet across the structure. This couplet is well modeled by elastic dislocation theory if the rake is in the range −110 to −150° (Figure 12d), i.e., if it has a greater component of normal motion than suggested by the GCMT mechanism (rake −165°). Using the GCMT rake, the predicted deformation pattern develops line-of-sight quadrants (Figure 12c) in place of the couplet. The aftershock interferogram has a negative (blue) lobe to the east of the positive (red) lobe, which is suggestive of a quadrant pattern. However, such a pattern is absent from any of the post-aftershock images, three of which are independent, and so the negative lobe in the aftershock image is likely an artifact resulting from tropospheric water vapor. We therefore suggest that the aftershock rake is in the range −110 to −150° and that the GCMT rake is inaccurate by up to a few tens of degrees, which as shown by *Weston et al.* [2011] is the range of differences between InSAR and CMT rake for earthquakes globally. In summary, our interpretation of the deformation across the hanging wall structure is that it is a steeply dipping release fault which slipped with a combination of extensional motion (possibly dominant) and right-lateral motion.

[19] Since release faults represent a response to a specific type of fault displacement geometry, it is likely that such

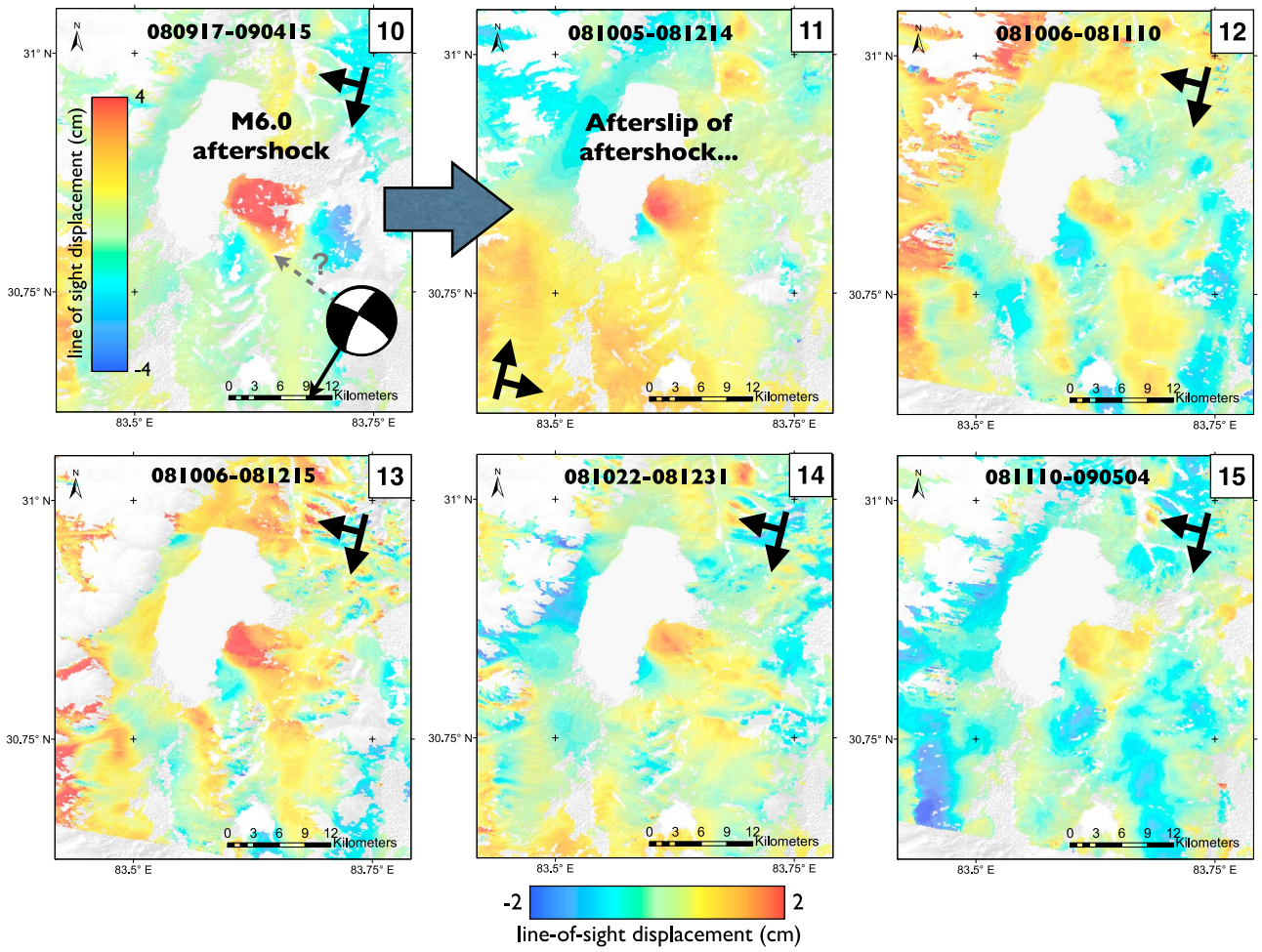


**Figure 11.** Unwrapped postseismic interferograms for the 2008 Zhongba earthquake. Start and end dates are given in yymmdd format at the top of each image, and numbers in the top right of each image correspond to those in Table 1. Interferogram 10 covers the Mw 6.0 aftershock on 25 September 2008, while 11–15 post-date this aftershock. The aftershock focal mechanism shown with interferogram no. 10 is from the Global CMT catalog. The black arrow points to the GCMT location and the gray dashed arrow with question mark indicates where, according to our interpretation, the aftershock occurred.

structures develop as displacement accumulates on an individual fault over repeated earthquake cycles, rather than being pre-existing features inherited from an older tectonic regime. The correlation of the release fault with a small zone of positive Coulomb stress change (see Section 4.2) further supports this idea. There may be other release faults in this same hanging wall valley. For example, the eastern "arm" of the hanging wall lake that juts out may be a result of previous offset on another release structure, perhaps a SW-dipping structure in the northern part of the hanging wall. Over time, this would act as a complement to the release deformation observed in the present study.

### 6.3. Normal Fault Sequences in Tibet

[20] Cross-referencing the earthquake catalogs from the National Earthquake Information Centre (NEIC) and the Global CMT project indicates that there have been other sequences of normal faulting events on the Tibetan Plateau over the last 40 years. Figure 17 plots magnitude against time for M > 4.5 earthquakes within six different areas on the Plateau where normal faulting events have occurred. All areas are collapsed onto the same time axis. The top plot is for 1980–2006 and the lower plot is for 2008, since several earthquakes occurred in this year alone. What is notable is that in five of the six areas, the largest earthquakes within a given grouping are within one magnitude point of each other, as marked by the boxes in Figure 17. We use the term "duo" when the two largest events are within one magnitude point, "trio" when the three largest events are, and "swarm" when several events are clustered in magnitude.

[21] The most striking example of magnitude clustering is in the earthquake swarms that occurred in 1996 and 1998 in the Pumqu-Xianza Rift. In the first swarm, five earthquakes with clustered magnitudes (4.9–5.7) occurred within two months of each other in July through August 1996. In the second swarm, seven earthquakes with magnitudes 5.0–5.8 occurred within a three-month period in July to October 1998. Less intense clustering occurred in the duos at Yari (1982), Zhongba (2005), Zhongba (2008) and Damxung (2008), and in the trio at Nima (2008). The only earthquake

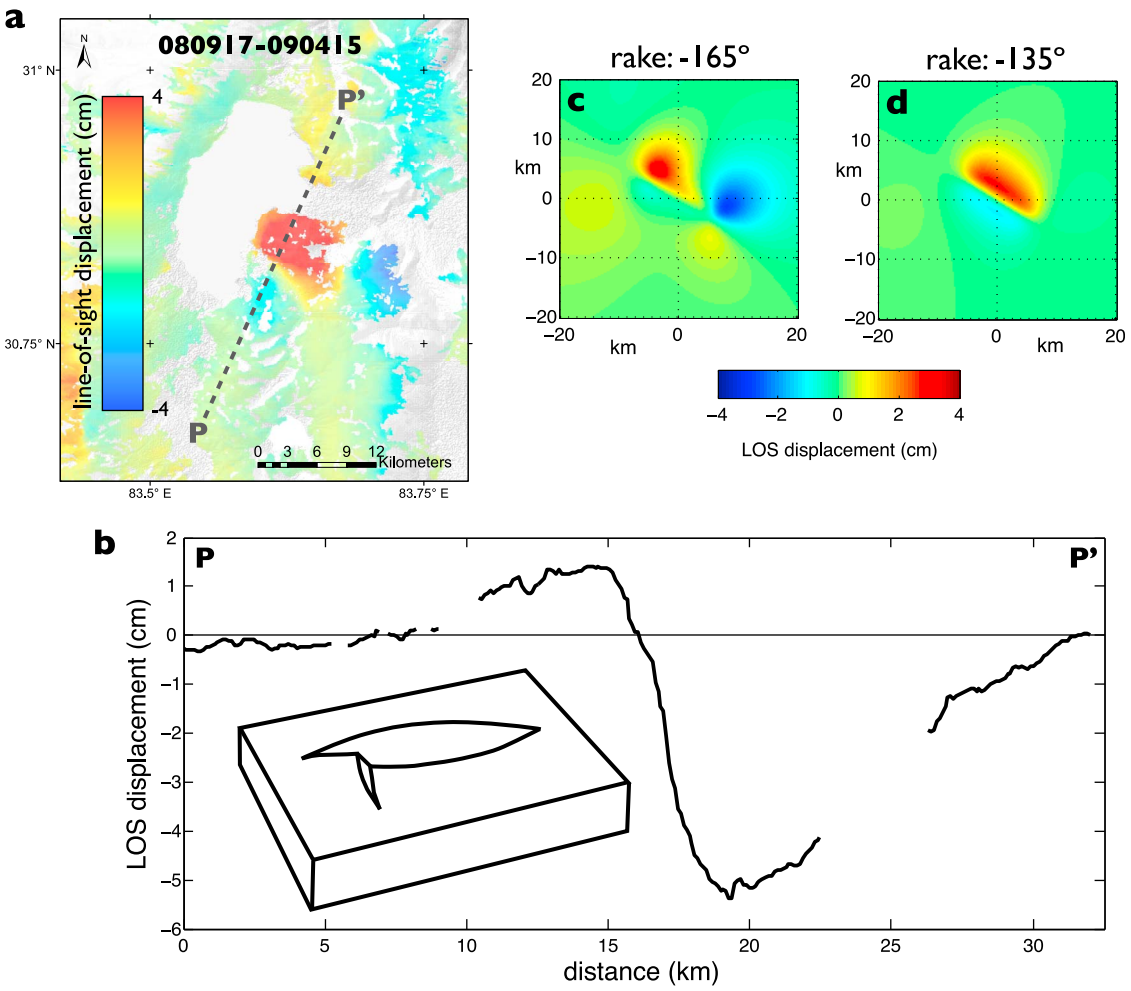


**Figure 12.** (a) Interferogram 10 reproduced for reference to accompanying panels. (b) Line-of-sight displacement profile across the hanging wall release fault, showing displacements that occurred during the Mw 6.0 aftershock (plus some afterslip). The profile is displayed with positive and negative reversed relative to the interferogram images, in order to give a sense of vertical displacement. The inset schematic diagram [after *Destro*, 1995] shows the relationship between the main 2008 Zhongba fault and its hanging wall release fault. (c, d) Forward-modeled displacements for the aftershock, projected into Envisat descending line-of-sight, for two different rake values.

for which all aftershocks are at least an order of magnitude smaller than the main shock, and which is not part of a longer sequence, is the 2008 Yutian earthquake in the NW part of the Plateau. For comparison, we note that for the two large strike-slip earthquakes that occurred on the Plateau at Manyi (Mw 7.5) and Kokoxili (Mw 7.9) in 1997 and 2001 respectively, the largest aftershocks were two orders of magnitude smaller than the main shock. The purpose of this paper is not to explore magnitude distributions in the context of Bath's Law, but rather to emphasize that grouped extensional events of moderate size, within a small magnitude range, are common on the Tibetan Plateau. Clustering may occur in a short time period (e.g., the Yari and Damxung duos, the Nima-Gaize trio), or across a several year window, with each main event having its own sub-cluster (the Zhongba sequence, the Pumqu swarms).

[22] Of the groupings referred to above, the Nima-Gaize trio has been well studied [*Sun et al.*, 2008; *Ryder et al.*, 2010; *He and Peltzer*, 2010]. This earthquake sequence is an interesting example to examine in light of the generalized triggering models presented in Section 5. Within a two-week period, Mw 6.4, 5.9 and 5.4 earthquakes occurred in close spatial proximity. InSAR images of the two larger events indicate that two synthetic faults ruptured, the second one in the hanging wall of the first, about 7 km away trace-to-trace, and in the top few km of the crust. *He and Peltzer* [2010] carried out detailed stress calculations for this event, including time-variable pore pressure, and found that the large aftershock was located in a zone of positive Coulomb stress change.

### 6.4. Normal Fault Sequences Outside of Tibet

[23] Outside of Tibet, there are several examples of extensional systems in which groups of faults have ruptured closely in space and time, similar to the Tibet cases discussed above. *Jackson et al.* [1982] studied the 1981 sequence in the Gulf of Corinth, a graben structure within

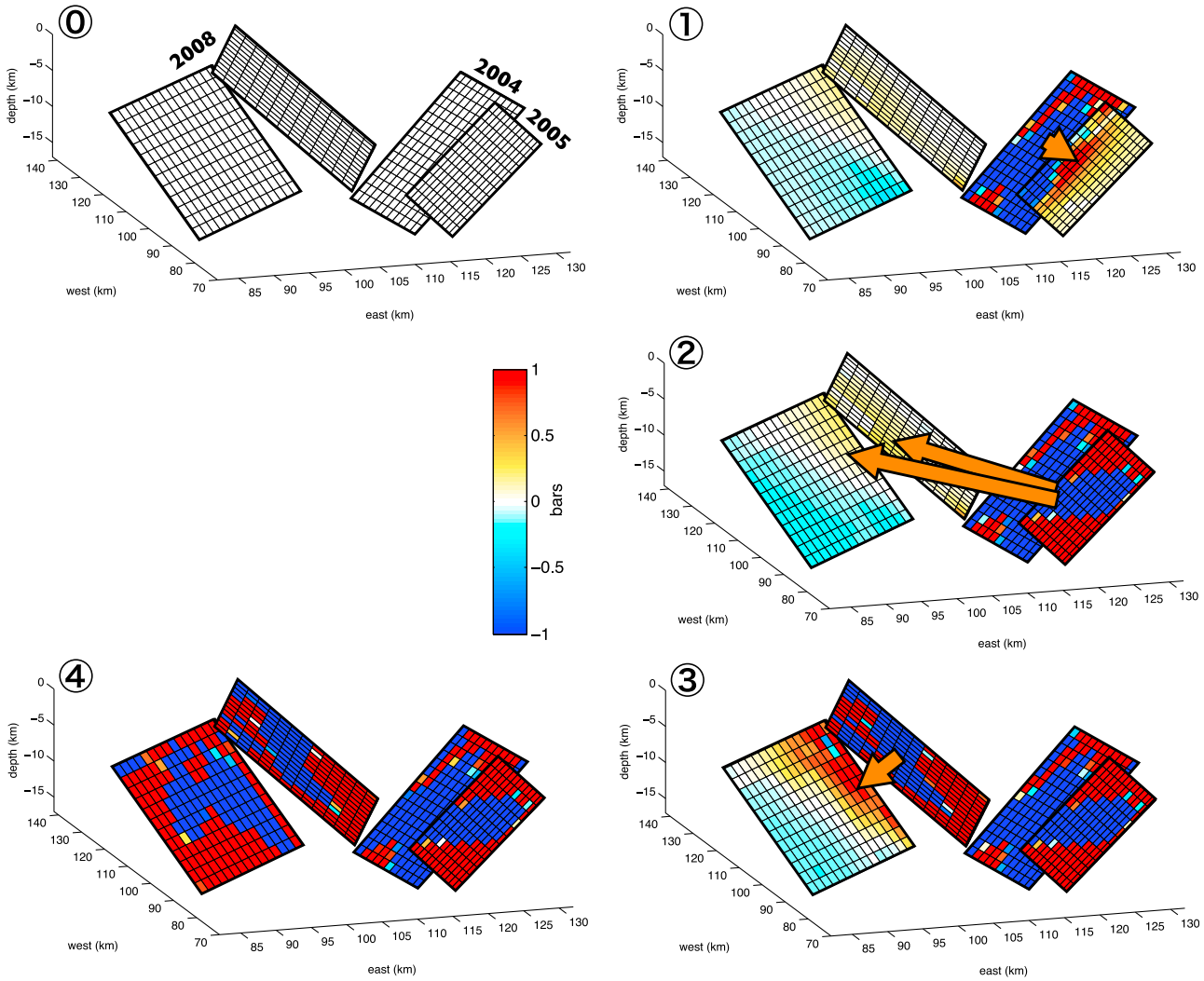


**Figure 13.** Results of Coulomb stress calculations described in Section 4. Colors show Coulomb stress changes resolved onto the various faults, with the rake for each fault patch as shown by the slip vectors in Figure 8. Different stages of the Zhongba sequence are numbered 0 (prior to any earthquakes) to 4 (all three earthquakes have occurred). Orange arrows give a sense of where positive stresses are transferred by successive ruptures.

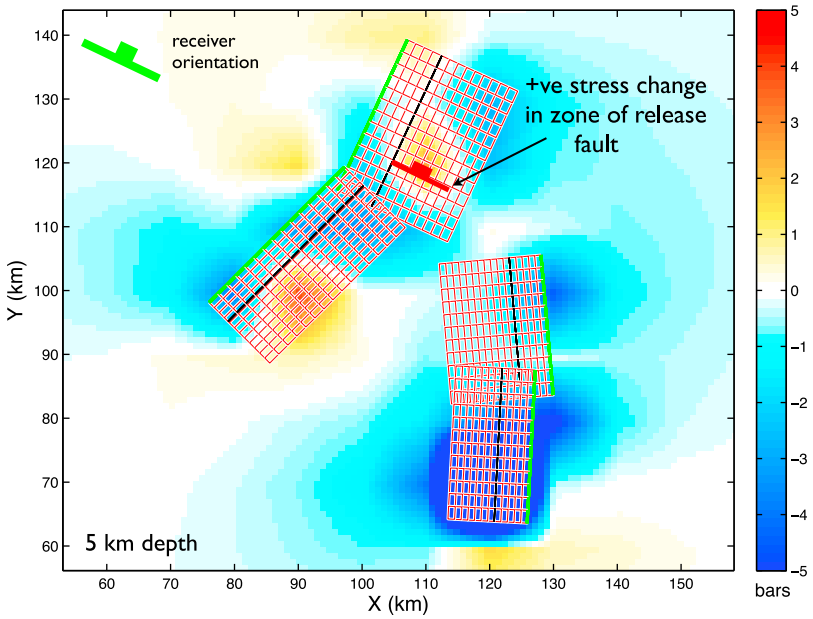


**Figure 14.** Results of Coulomb stress calculation for the hanging wall release fault. Calculations were carried out for a depth of 5 km (the estimated middle depth of the release fault) and a receiver fault geometry corresponding to the Global CMT focal mechanism: strike 302°, dip 77°, rake −165°. The green lines are the fault traces of the Zhongba main shocks and the red rectangles mark the patches on each fault. Black lines indicate where the horizontal section intersects each fault at 5 km depth. A positive stress change occurred in the zone of the release fault (red line).

the extensional regime of central Greece. Three earthquakes with Ms 6.7, 6.4 and 6.4 ruptured across the gulf within a two-week period in 1981. The first and second events ruptured north-dipping faults on the south side of the gulf, along strike from each other, and the third event ruptured a diagonally opposite south-dipping fault on the other side of the graben. The sequence is therefore consistent with the triggering scenarios described in Section 5. *Nostro et al.* [1997] studied the 1980 Irpinia earthquake, which consisted of four sub-events that occurred within 40 s of each other, and concluded that successive sub-events were triggered by static stress changes from previous sub-events. In 1997 the Umbria-Marche earthquake sequence occurred in the northern Apennines of Italy. The three largest shocks (Mw 5.7, 6.0, 5.7) ruptured a series of three SW-dipping faults alongstrike from each other, beginning with the central fault [*Cinti et al.*, 1999]. A similar sequence occurred in L'Aquila in the Abruzzi region of central Italy in 2009, with three SW-dipping faults rupturing in the three largest events (Mw 6.3, 5.4, 5.5), again starting from the central fault [*Pondrelli et al.*, 2010; *Mariucci et al.*, 2010]. The 1954 Basin and Range earthquake sequence that ruptured the Rainbow Mountain, Fairview Peak and Dixie Valley faults [*Hodgkinson et al.*, 1996] is not, in spite of occurring in one of the classic extensional regions of the world, a classic pure normal faulting scenario. The first two Rainbow Mountain earthquakes are estimated to have had a much greater component of strike slip than dip slip [*Hodgkinson et al.*, 1996], and the Dixie Valley event was also markedly oblique. Furthermore, several earlier earthquakes occurred in the vicinity of the 1954 sequence in the first half of the twentieth century. Because of these complications, we do not attempt to compare this sequence against the generalized patterns presented in Section 5, but we note that *Hodgkinson et al.* [1996] carry out a detailed study of stress changes during the 1954 sequence and concluded that later events were triggered by static stress changes from earlier events.

[24] Normal faulting sequences have also been recorded in an entirely different tectonic setting. InSAR images of the Iwaki sequence, consisting of six events with Mw 5.4–6.6, in coastal Japan in March–April 2011 following the great Tohoku-Oki earthquake clearly show that events later in the sequence ruptured faults in the hanging walls of earlier events (http://www.geerassociation.org/GEER_Post%20EQ%20Reports/Tohoku_Japan_2011/Quick%20Report_4_index.html). It should be noted that the entire area in which this swarm occurred was positively stressed by a massive amount as a result of slip on the megathrust, and any local reduction in stress during the sequence was minor in comparison. The entire Iwaki sequence can therefore be regarded as having been triggered by the Tohoku-Oki earthquake. The Pichilemu normal faulting aftershocks of the 2010 Maule earthquake [*Farias et al.*, 2011; *Ryder et al.*, 2012] occurred in a similar tectonic setting to the Iwaki sequence, i.e., in a region of large stress change following a megathrust rupture. However, the Pichilemu sequence is potentially different in that the two "main" events (Mw 6.9 and 6.7) occurred within 15 min of each other, and so dynamic stresses may have played an important role in the triggering of the second event.

### 6.5. Phase Locking of Fault Ruptures

[25] A question that arises in connection with earthquake sequences is whether or not the sequences themselves are a persistent phenomenon, recurring at time intervals much longer than the time between individual events within a sequence. Although calculations of Coulomb stress change

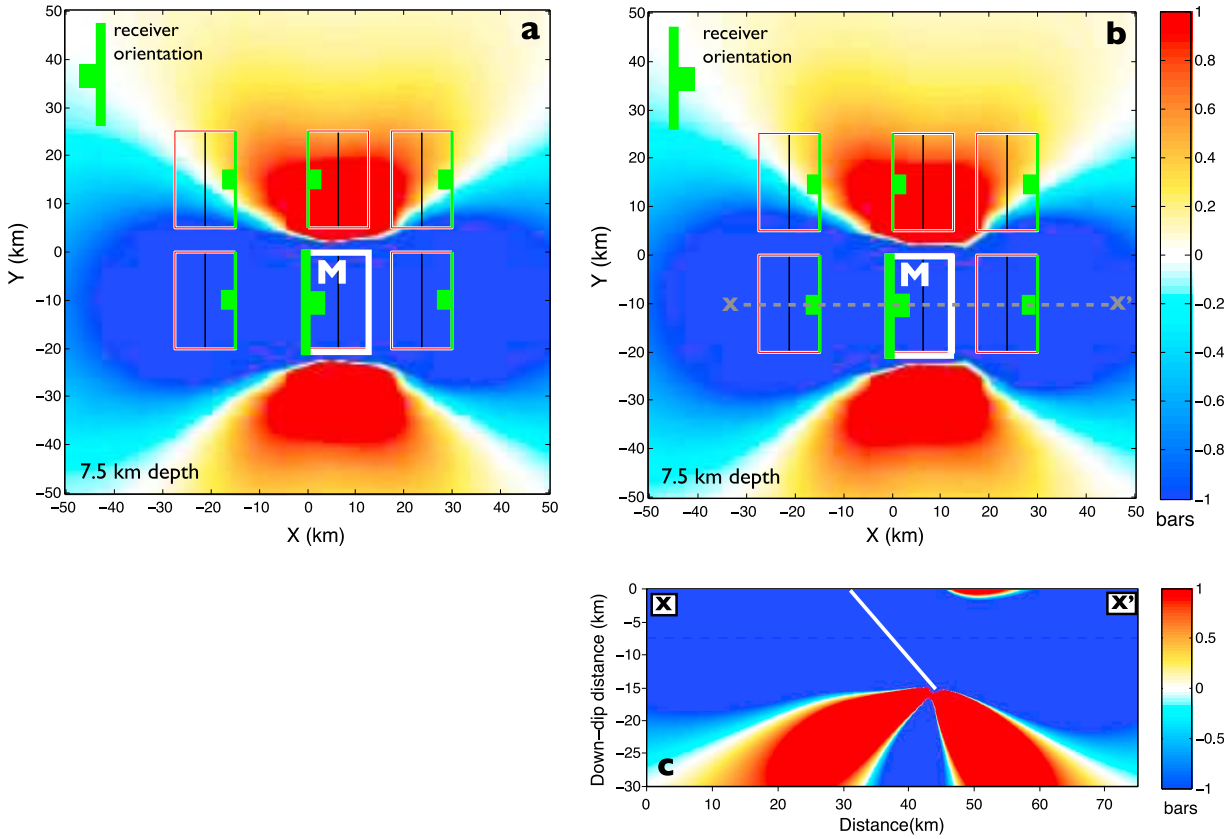


**Figure 15.** Results of generalized Coulomb stress calculations for an idealized Zhongba-like system with NS-striking faults dipping at 50°. In top two panels, green lines mark fault traces and white boxes are projections of the fault outlines to the surface. Black lines indicate the calculation depth of 7.5 km. The master fault that slips is marked by the letter M. (a) The receiver fault is antithetic to the master fault. (b) The receiver fault has the same orientation as the master fault. Dashed gray line (X-X′) shows location of cross section in Figure 15c. (c) Cross section showing Coulomb stress change due to slip on the master fault, for a receiver fault geometry identical to that of the master fault.

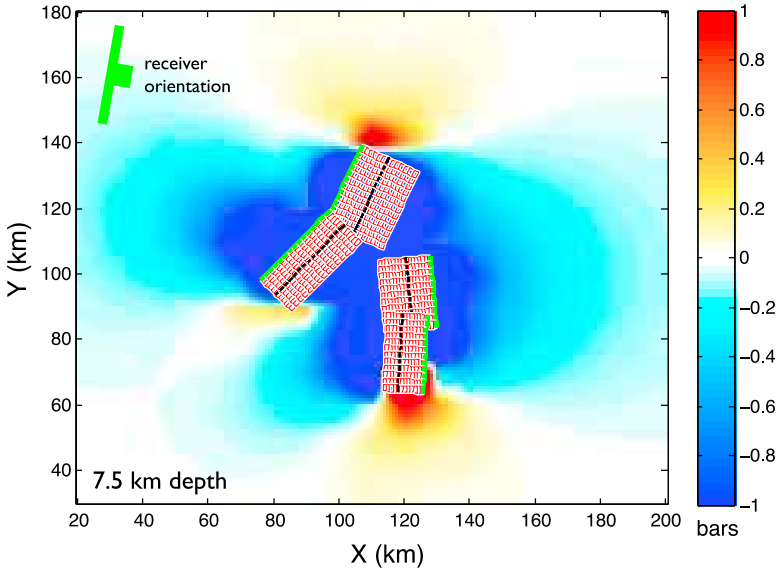


**Figure 16.** Results of Coulomb stress calculations for the Zhongba sequence, showing the total stress changes resulting from all three earthquakes, for a receiver fault geometry as follows: strike 30°, dip 45°, rake −90°. Green lines mark fault traces and white boxes are projections of the fault outlines to the surface. Black dashed lines indicate the calculation depth of 7.5 km.

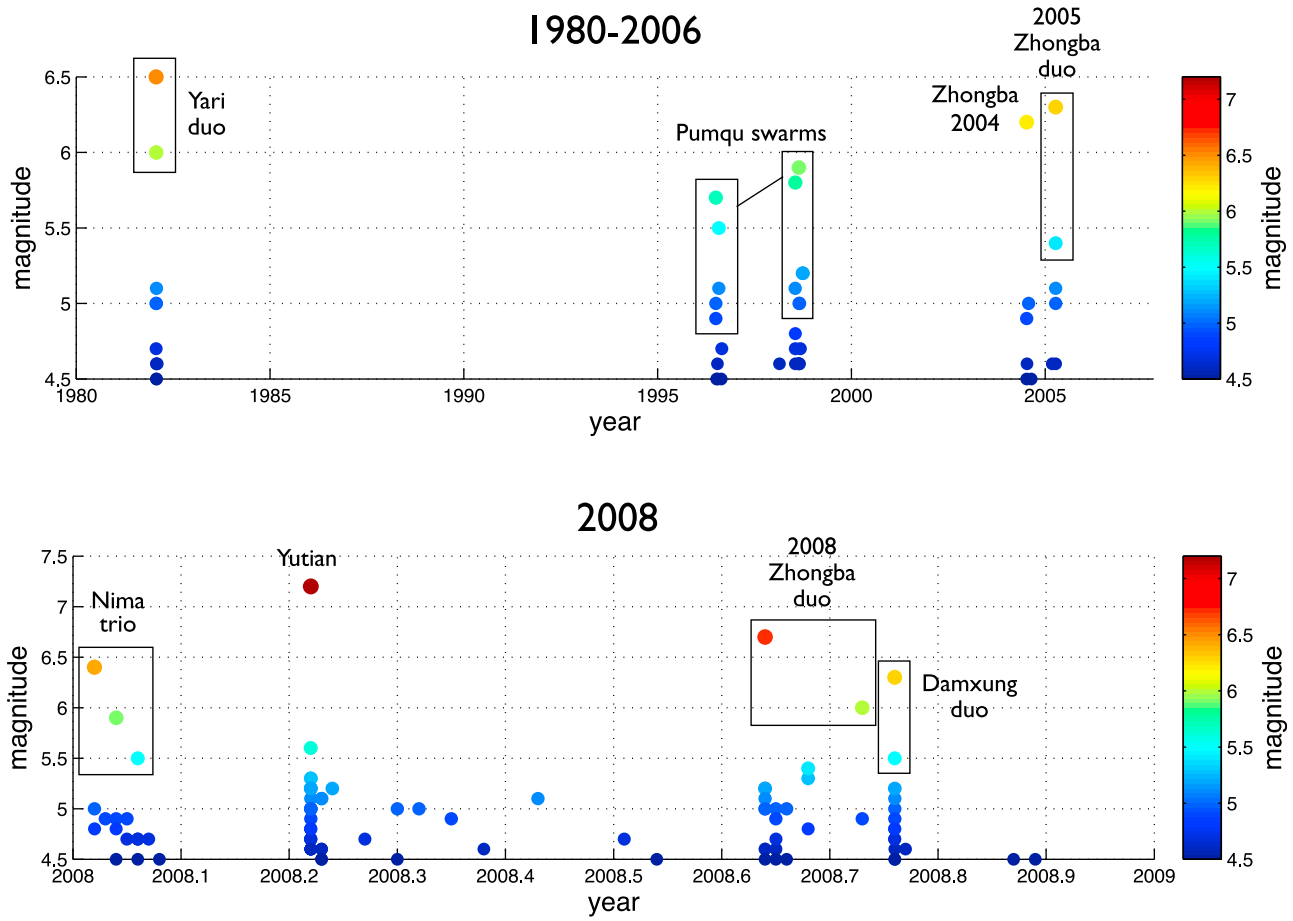


**Figure 17.** Magnitude plotted against time for earthquakes in different areas of the Tibetan Plateau. As well as the *y* axis being magnitude, the dots (denoting individual earthquakes) are colored by magnitude. Boxes indicate where earthquakes are clustered within a magnitude range of less than 1.

can suggest which parts of a system have been brought closer to failure, and by how much, whether or not a fault is near the end of its earthquake cycle is also an important factor. *Scholz* [2010] suggested and explored the idea that proximal faults with similar slip rates can become synchronized, such that they always rupture at approximately the same time as each other. The physical mechanism behind such phase locking is that static stress increases associated with a slipped fault bring nearby faults closer to the end of their earthquake cycle, and over time the cycles on different faults become temporally aligned. Since faults would be approaching the end of their cycle simultaneously, a small stress change resulting from rupture on one of them may easily trigger a rupture on another. In the Zhongba case, for example, the stress perturbations on neighboring faults were much smaller (≤1 bar) than the stress drops in the earthquakes themselves (25–80 bars). Similar slip rates on faults are a requirement for phase locking to occur [*Scholz*, 2010]. Variable extension rates along the South Lunggar Rift [*Styron et al.*, 2011], coupled with the more distributed style of faulting in the southern part, may mean that the Zhongba sequence will not continue beyond 2008. For groups of faults with low slip rates that host moderate-sized earthquakes, such as the Zhongba group, one would have to observe the system for many centuries in order to verify whether fault synchronization is a physical reality, rather than a one-off coincidence. Instead, phase locking may be explored by consideration of groups of smaller faults with much shorter earthquake cycles.

## 7. Conclusions

[26] In this paper we have carried out a detailed analysis of the Zhongba earthquake sequence in the South Lunggar Rift zone, SW Tibet, in terms of fault geometry, slip distribution and static stress changes. The sequence is consistent with triggering by static stress transfer, both in terms of the spatial pattern of successive earthquakes and also the order in which they occurred. This paper documents for the first time active displacement across a hanging wall release fault, during the Mw 6.0 aftershock of the 2008 Zhongba earthquake. Like the main shocks, the release aftershock is shown to be fully consistent with triggering by static stress transfer. While it is not clear whether the Zhongba sequence will continue, if it does, the most likely fault to rupture next is the northern continuation of the one that failed in 2008. Normal faulting sequences in which several moderate-sized (M 5.5–7) earthquakes occur close in space, time and magnitude are not uncommon, and there are several well-documented examples from the Tibetan Plateau and elsewhere in the world.

[27] **Acknowledgments.** This research was started as part of NSF grant EAR-1014880. Envisat data are copyright ESA and were obtained through ESA Category-1 award C1P.5119 and ESA AO 668. Part of this research was sponsored by the NASA Earth Science and Interior Focus Area and performed at the Jet Propulsion Laboratory, California Institute of Technology, Pasadena, California. Several figures in this paper were produced using the Coulomb software (version 3.2.01), and Figure 1a was produced using GeoMapApp (version 3.1.6).

## References

Cinti, F., L. Cucci, F. Marra, and P. Montone (1999), The 1997 Umbria-Marche (Italy) earthquake sequence: Relationship between ground deformation and seismogenic structure, *Geophys. Res. Lett.*, *26*(7), 895–898.

Destro, N. (1995), Release faults: A variety of cross fault in linked extensional fault systems in the Sergipe-Alagoas Basin, NE Brazil, *J. Struct. Geol.*, *17*, 615–629.

Elliott, J. R., R. J. Walters, P. C. England, J. A. Jackson, Z. Li, and B. Parsons (2010), Extension on the Tibetan plateau: Recent normal faulting measured by InSAR and body wave seismology, *Geophys. J. Int.*, *183*, 503–535.

Farias, M., D. Comte, S. Roecker, D. Carrizo, and M. Pardo (2011), Crustal extensional faulting triggered by the 2010 Chilean earthquake: The Pichilemu Seismic Sequence, *Tectonics*, *30*, TC6010, doi:10.1029/2011TC002888.

Farr, T. G., et al. (2007), The Shuttle Radar Topography Mission, *Rev. Geophys.*, *45*, RG2004, doi:10.1029/2005RG000183.

Freed, A. M. (2005), Earthquake triggering by static, dynamic, and post-seismic stress transfer, *Annu. Rev. Earth Planet. Sci.*, *33*, 335–367, doi:10.1146/annurev.earth.33.092203.122505.

Goldstein, R. M., H. A. Zebker, and C. L. Werner (1988), Satellite radar interferometry: Two-dimensional phase unwrapping, *Radio Sci.*, *23*, 713–720.

He, J., and G. Peltzer (2010), Poroelastic triggering in the 9–22 January 2008 Nima-Gaize (Tibet) earthquake sequence, *Geology*, *38*(10), 907–910, doi:10.1130/G31104.1.

Hodgkinson, K. M., R. Stein, and G. C. P. King (1996), The 1954 Rainbow Mountain-Fairview Peak-Dixie Valley earthquakes: A triggered normal faulting sequence, *J. Geophys. Res.*, *101*(B11), 25,459–25,471, doi:10.1029/96JB01302.

Jackson, J. A., J. Gagnepain, G. Houseman, G. C. P. King, P. Papadimitriou, C. Soufleris, and J. Virieux (1982), Seismicity, normal faulting, and the geomorphological development of the Gulf of Corinth (Greece): The Corinth earthquakes of February and March 1981, *Earth Planet. Sci. Lett.*, *57*(2), 377–397.

Kapp, P., M. Taylor, D. Stockli, and L. Ding (2008), Development of active low-angle normal fault systems during orogenic collapse: Insight from Tibet, *Geology*, *36*, 7–10, doi:10.1130/G24054A.1.

King, G. C. P., R. S. Stein, and J. Lin (1994), Static stress changes and the triggering of earthquakes, *Bull. Seismol. Soc. Am.*, *84*(3), 935–953.

Lin, J., and R. S. Stein (2004), Stress triggering in thrust and subduction earthquakes and stress interaction between the southern San Andreas and nearby thrust and strike-slip faults, *J. Geophys. Res.*, *109*, B02303, doi:10.1029/2003JB002607.

Mariucci, M. T., P. Montone, and S. Pierdominici (2010), Present-day stress in the surroundings of 2009 L'Aquila seismic sequence (Italy), *Geophys. J. Int.*, *182*, 1096–1102, doi:10.1111/j.1365-246X.2010.04679.x.

Nostro, C., M. Cocco, and M. E. Belardinelli (1997), Static stress changes in extensional regimes: An application to Southern Apennines (Italy), *Bull. Seismol. Soc. Am.*, *87*(1), 234–248.

Pondrelli, S., S. Salimbeni, A. Morelli, G. Ekström, M. Olivieri, and E. Boschi (2010), Seismic moment tensors of the April 2009, L'Aquila (central Italy), earthquake sequence, *Geophys. J. Int.*, *180*, 238–242, doi:10.1111/j.1365-246X.2009.04418.x.

Rosen, P. A., S. Hensley, G. Peltzer, and M. Simons (2004), Updated repeat orbit interferometry package released, *Eos Trans. AGU*, *85*(5), 47, doi:10.1029/2004EO050004.

Ryder, I., R. Burgmann, and J. Sun (2010), Tandem afterslip on connected fault planes following the 2008 Nima-Gaize (Tibet) earthquake, *J. Geophys. Res.*, *115*, B03404, doi:10.1029/2009JB006423.

Ryder, I., R. Rietbrock, K. Kelson, and R. Burgmann (2012), Large extensional aftershocks in the continental forearc triggered by the 2010 Maule earthquake, Chile, *Geophys. J. Int.*, *188*(3), 879–890, doi:10.1111/j.1365-246X.2011.05321.x.

Scholz, C. (2010), Large earthquake triggering, clustering, and the synchronization of faults, *Bull. Seismol. Soc. Am.*, *100*(3), 901–909.

Styron, R., M. H. Taylor, D. F. Stockli, K. E. Sundell, A. T. McCallister, L. Ding, and D. Liu (2011), The South Lunggar Rift, Western Tibet: Rates, timing and evolution of an active detachment system from structural mapping and (U-Th)/He thermochronology, paper presented at 2011 Annual Meeting, Geol. Soc. Am., Minneapolis, Minn., 9–12 Oct.

Sun, J., Z. Shen, X. Xu, and R. Burgmann (2008), Synthetic normal faulting of the 9 January 2008 Nima (Tibet) earthquake from conventional and along-track SAR interferometry, *Geophys. Res. Lett.*, *35*, L22308, doi:10.1029/2008GL035691.

Taylor, M., and A. Yin (2009), Active structures of the Himalayan-Tibetan orogen and their relationships to earthquake distribution, contemporary strain field, and Cenozoic volcanism, *Geosphere*, *5*(3), 199–214.

Weston, J., A. Ferreira, and G. Funning (2011), Global compilation of interferometric synthetic aperture radar earthquake source models: 1. Comparisons with seismic catalogs, *J. Geophys. Res.*, *116*, B08408, doi:10.1029/2010JB008131.